Image Cover Sheet

CLASSIFICATION	SYSTEM NUMBER
UNCLASSIFIED	510321

TITLE

THE EFFECT OF CRACK TIP RADIUS ON INITIATION FRACTURE TOUGHNESS

System Number:

Patron Number:

Requester:

Notes: Paper #16 contained in Parent Sysnum #510305

DSIS Use only:

Deliver to: DK

#510321 (16)

THE EFFECT OF CRACK TIP RADIUS ON INITIATION FRACTURE TOUGHNESS

Ken MacKay[1], Ken KarisAllen[2], G.M.C. Lee[1]

[1]Department of Mining and Metallurgy
Technical University of Nova Scotia
P.O. Box 1000, Halifax, Nova Scotia
Canada, B3J 2X4

[2] Dockyard Laboratory
Defence Research Establishment Atlantic
P.O. Box 1012, Dartmouth, Nova Scotia
Canada, B2Y 3Z7

Abstract

Fracture standards maximize crack tip constraint by including a mandatory fatigue precracking procedure prior to determining initiation fracture toughness. This procedure is time consuming and may introduce considerable scatter and uncertainty in the determined toughness values. A mechanical or electrical means of manufacturing defects would provide a significant economic benefit as well as a more reproducible initial crack tip profile. The objective of this research is to evaluate various alternative methods of producing defects by determining the relationship between lower bound initiation fracture toughness and crack tip radius. A review of the literature indicates that a critical crack tip radius exists below which the apparent fracture toughness becomes independent of any further decrease in radius. Preliminary tests using low alloy steel fatigue precracked specimens (a/W = 0.60) and electric discharge machining (EDM) notched specimens (a/W = 0.45, with crack tip radii 60 -75 mm) generate average apparent toughness values of 232 kJ/m^2 and 400 kJ/m^2, respectively. EDM notched specimens provide greater reproducibility of the apparent toughness values compared to the fatigue precracked specimens. From the limited data obtained to date, it is uncertain whether the increase in toughness for the a/W = 0.45 specimens results from the decrease in crack depth or from the increase in crack tip radius.

Introduction

Current ASTM fracture standards [1] maximize crack tip constraint by including a mandatory fatigue precracking procedure prior to determining initiation fracture toughness. In general, the apparent toughness increases as the crack tip radius increases. Therefore, a fatigue crack gives a conservative value of the J-integral since the crack tip radius for a fatigue crack approaches zero. This procedure is time consuming and may introduce considerable scatter and uncertainty in the determined toughness value. Much of the uncertainty is due to the lack of reproducibility in the crack tip profile owing to slight differences in applied loading and material variation across the crack front (a particular problem with welded specimens) during the fatigue precracking. A reproducible mechanical or electrical means of creating defects with finite crack tip radii could replace fatigue precracking if a relationship between the lower bound initiation fracture toughness and crack tip radius existed.

Background

For linear-elastic material, the stresses near a sharp crack ($r \rightarrow 0$) in an infinite plate subjected to a tensile stress σ are [2, 3, 4]:

$$\sigma_x = \sigma\sqrt{\frac{\pi a}{2\pi r}} \cdot \cos\frac{\theta}{2}\left[1-\sin\frac{\theta}{2}\sin\frac{3\theta}{2}\right] \quad (1)$$

$$\sigma_y = \sigma\sqrt{\frac{\pi a}{2\pi r}} \cdot \cos\frac{\theta}{2}\left[1+\sin\frac{\theta}{2}\sin\frac{3\theta}{2}\right] \quad (2)$$

$$\tau_{xy} = \sigma\sqrt{\frac{\pi a}{2\pi r}} \cdot \sin\frac{\theta}{2}\cos\frac{\theta}{2}\cos\frac{3\theta}{2} \quad (3)$$

where the stress components and the polar coordinates are depicted in Figure 1. The above equations are only valid for $r<<a$. For plane stress conditions, $\sigma_z = 0$, and for plane strain conditions, $\sigma_z = \nu(\sigma_x + \sigma_y)$, where ν is Poisson's ratio. Equations 1, 2, and 3 show that the stresses near the crack tip are a function of position ($f(\theta) / (2\pi r)^{1/2}$) and a function of the remote stress and crack length ($\sigma(\pi a)^{1/2}$). The $\sigma(\pi a)^{1/2}$ term in Equations 1, 2, and 3 is defined as the stress intensity factor, K_I, for Mode I loadings.

Creager and Paris [5] developed a similar set of equations for a crack with a finite tip radius:

$$\sigma_x = \frac{K_I}{\sqrt{2\pi r}} \cdot \cos\frac{\theta}{2}\left[1-\sin\frac{\theta}{2}\sin\frac{3\theta}{2}\right] - \frac{K_I}{\sqrt{2\pi r}} \cdot \frac{\rho}{2r}\cos\frac{3\theta}{2} \quad (4)$$

$$\sigma_y = \frac{K_I}{\sqrt{2\pi r}} \cdot \cos\frac{\theta}{2}\left[1+\sin\frac{\theta}{2}\sin\frac{3\theta}{2}\right] + \frac{K_I}{\sqrt{2\pi r}} \cdot \frac{\rho}{2r}\cos\frac{3\theta}{2} \quad (5)$$

$$\tau_{xy} = \frac{K_I}{\sqrt{2\pi r}} \cdot \sin\frac{\theta}{2}\cos\frac{\theta}{2}\cos\frac{3\theta}{2} - \frac{K_I}{\sqrt{2\pi r}} \cdot \frac{\rho}{2r}\cos\frac{3\theta}{2} \quad (6)$$

The origin of the polar coordinate system for Equations 4, 5, and 6 is half the root radius away from the crack tip, as shown in Figure 2. For a blunted crack the stress at the crack tip is finite, whereas the stresses at the tip of a sharp crack approach infinity (i.e. there is no crack tip singularity in the case of the blunted crack). For $\rho = 0$, Equations 4, 5, and 6 reduce to Equations 1, 2, and 3 for the stress fields for sharp crack.

Equations 4 through 6 show that the stress distribution ahead of a crack is affected by the crack tip radius. For plane strain conditions, an increase in crack tip radius decreases the maximum value of σ_y and moves the position of the maximum towards the elastic-plastic boundary as shown in Figure 3 [2, 6, 7]. This change in the stress distribution is due to a

reduction in the triaxiality at the crack tip brought about by the increased free surface at the blunted crack tip. For perfectly elastic-plastic materials, the stress in the plastic zone is given by [7, 8]:

$$\sigma_y = \sigma_{ys}\left(1+\ln\left(1+\frac{X}{\rho}\right)\right) \tag{7}$$

using Tresca yield criterion and taking the origin at the crack tip (see Figure 3). The maximum value of σ_y, given by Equation 7, occurs at the elastic-plastic interface.

Several studies have been conducted on the relationship between root radius and apparent fracture toughness [6, 9, 10, 11 - 17]. These studies conclude that, in general, the apparent fracture toughness, J_{IA}, decreases as the crack tip radius decreases until a limiting value of $\rho = \rho_c$ is reached. Below this limiting value, the apparent fracture toughness becomes independent of crack tip radius.

Xiulin [18] derived equations for the elastic and elastic-plastic fracture toughness based on notch strain analysis and strain fracture criterion for ductile materials under plane strain conditions as:

$$K_{IA} = 0.32\sqrt{\pi E \sigma_f \varepsilon_f \rho} \tag{8}$$

and

$$J_{IA} = 0.1(1-\nu^2)\pi \sigma_f \varepsilon_f \rho \tag{9}$$

where σ_f is the critical fracture stress and ε_f is the fracture strain. When the crack tip radius decreases to the critical value ρ_c, the fracture toughness is described by:

$$J_{IC} = 0.1(1-\nu^2)\pi \sigma_f \varepsilon_f \rho_c \tag{10}$$

The value of ρ_c was determined to be a constant which depended on the microstructure of the material. For low alloy high strength steels, ρ_c is approximately equal to the spacing between inclusions [12, 16, 18]. Xiulin discovered that for steel with a martensitic microstructure, the value of ρ_c depended upon the type of martensite present. For high strength steels of lath martensite, and also for aluminum alloys, the value of ρ_c was equal to the strain hardening exponent, n, in mm. For high strength steels with a mixed martensite microstructure, ρ_c was equal to the uniform elongation, δ_b, in mm, or the prior austenite grain diameter, or 9 times the diameter of the dimples found on the ductile fracture surface [18]. For AISI 4340 steel with a martensite microstructure, the value of ρ_c was found to be the grain diameter of prior austenite [18]. Xiulin compared experimental toughness values found in the literature with those calculated using Equation 9. For twelve alloy steels, each tempered to different levels of toughness, and for four aluminum alloys, the difference between the experimental values and the calculated values was less than 10%. Since the dimple size and uniform elongation increase with toughness, ρ_c is also expected to increase with fracture toughness. The increase in ρ_c with fracture toughness has already been implied by Equations 9 and 10.

The results of Xiulin are based on ductile fracture. However, similar models have been proposed for brittle fracture in low alloy steels. Ritchie and Horn [6] proposed that the apparent fracture toughness for stress controlled fracture (intergranular cleavage and quasicleavage) is:

$$K_{IA} \approx 2.9\sigma_{ys}\sqrt{\rho\left[\exp\left(\frac{\sigma_f}{\sigma_{ys}}-1\right)-1\right]} \tag{11}$$

$$J_{IA} \approx 8.4\sigma_{ys}^2\rho\left[\exp\left(\frac{\sigma_f}{\sigma_{ys}}-1\right)-1\right] \tag{12}$$

Using the critical crack tip radius ρ_c, the fracture toughness is given by:

$$K_{IC} \approx 2.9\sigma_{ys}\sqrt{\rho_c\left[\exp\left(\frac{\sigma_f}{\sigma_{ys}}-1\right)-1\right]} \tag{13}$$

$$J_{IC} \approx 8.4\sigma_{ys}^2\rho_c\left[\exp\left(\frac{\sigma_f}{\sigma_{ys}}-1\right)-1\right] \tag{14}$$

Equations 13 and 14 again indicate that the critical root radius increases as fracture toughness increases. Experimental results show that an increase in ρ_c is accompanied by an increase in toughness for as-quenched AISI 4340 steel austenitized at different temperatures where fracture occurred by quasicleavage [10]. Similar results have been observed for a mild steel and for an HSLA steel where fracture occurred by cleavage [13].

This report describes an experimental investigation into the relationship between lower bound initiation fracture toughness and crack tip radius. The objective is to determine the initiation fracture toughness where the toughness determined using specimens with finite crack tip radius deviates from the toughness determined in accordance with ASTM standard E813-89 [1]. The hypothesis is that the initiation fracture toughness decreases as the limiting crack tip radius decreases. Thus, for a given finite crack tip radius, a lower bound initiation fracture toughness should exist above which the apparent fracture toughness equals the initiation fracture toughness.

Experimental Program

Two sets of single edge notched three-point-bend specimens were machined from a 25 mm plate of HLES 80 in the T-L orientation. Detailed specimen dimensions are given in Table 1. The first set of specimens (a/W = 0.60) were fatigue precracked in accordance with ASTM E813-89. In the second set of specimens (a/W = 0.45), precracking was replaced by electric discharge machining slots. The crack tip radius for this manufactured defect is approximately 60-75 μm (0.0025 - 0.003 in.). All specimens were side grooved 10 percent

on each side to promote uniform crack extension across the crack front.

Quasi-static fracture tests were conducted on a computer controlled servo-hydraulic materials testing system. Periodic unloading compliance measurements were carried out to measure crack length in accordance with ASTM E-813. Initial and final 9 point average crack extension measurements were optically determined from the fracture surfaces subsequent to testing. Load and CMOD displacement data were collected and bussed to a microprocessor for storage and analysis.

For each specimen J-resistance curves were generated using the procedure outlined in ASTM E-813. The J-Δa data pairs were fitted to a power law function. J_{IC} was defined as the intersection of the 0.20 mm offset blunting line and fitted resistance data. Triplicate tests were performed for each specimen configuration.

Results and Discussion

Figures 4 and 5 show typical load displacement curves for each type of specimen. Figures 6 and 7 show plots of applied J vs Δa for a fatigue precracked specimen and an EDM notched specimen respectively. Both resistance curve data sets fit well to a power law function. The results of the tests are shown in Figure 8. The average apparent toughness value for the fatigue precracked specimens is 232 kJ/m^2. The two lower values for the fatigue precracked specimens are valid J_{IC} toughness values . The third toughness value is not valid due to insufficient crack extension. The average apparent toughness value for the EDM notched specimens is 400 kJ/m^2. This is significantly higher than the average apparent toughness determined from the fatigue precracked specimens. There are two possible explanations for this difference in the average apparent toughness values. The first possibility is that the crack tip radius of the EDM notched bars is greater than the limiting crack tip radius. The second factor is that there is a difference in crack depth between the fatigue cracked and EDM notched specimens. The shorter crack depths in the EDM notched specimens may be responsible for the difference in the apparent toughness values between the two specimen types.

There is less scatter in the apparent toughness values obtained from the EDM notched specimens. The range between the two valid toughness values obtained from the fatigue precracked specimens is 70 kJ/m^2. The range between the highest and lowest apparent toughness values obtained from the EDM notched specimens is 25 kJ/m^2. Thus, the use of the EDM notch improves the reproducibility of the determined toughness values compared to fatigue precracking. This improved reproducibility can be partially accounted for by the more uniform crack tip profiles produced using an EDM notch. Figure 9 compares the crack profiles of the fatigue precracked and EDM notched specimens. The fatigue precracked specimens extend a curved crack front with the leading edge near the surface of the side groove root. The EDM notched specimens start with a straight crack front which remains essentially straight during extension.

Conclusions

1) From a review of the literature, ρ_c was generally found to increase as the fracture toughness increased. While the value of ρ_c could be estimated from a number of material properties (e.g. inclusion spacing, uniform elongation, the prior austenite grain diameter, the strain hardening exponent, or the average dimple size on the ductile fracture surface), in each case the value of ρ_c increased as fracture toughness increased for low alloy steels in both the as-quenched and tempered conditions.

2) A significant difference exists between the apparent initiation fracture toughness determined using EDM notched specimens with a/W = 0.45 and using fatigue precracked specimens with a/W = 0.60. From the limited data obtained to date, it is uncertain whether the increase in toughness for the a/W = 0.45 specimens results from the decrease in crack depth or from the increase in crack tip radius.

3) Preliminary tests show that a machined notch of finite root radius provides improved reproducibility of the determined fracture toughness value, compared to fatigue precracking.

References

[1] "E813 Test Method for J_{IC}, A Measure of Fracture Toughness", Annual Book of ASTM Standards, Vol. 3.01, ASTM, Philadelphia, 1992.

[2] Ewalds, H.L., Wanhill, R.J.H., Fracture Mechanics, Edward Arnold, New York, 1989.

[3] Barsom, J.M., and McNicol, R.C., in "Fracture Toughness and Slow Stable Cracking", ASTM STP 559, American Society for Testing and Materials, Philadelphia, 1974, pp. 183-204.

[4] Irwin, G.R., "Analysis of Stresses and Strains Near the End of a Crack Traversing a Plate", Journal of Applied Mechanics, Vol. 24, 1957, pp. 361-364.

[5] Creager, M., and Paris, P.C., "Elastic Field Equations for Blunt Cracks with Reference to Stress Corrosion Cracking", International Journal of Fracture Mechanics, Vol. 3, 1967, pp. 247-252.

[6] Ritchie, R.O., and Horn, R.M., "Further Considerations on the Inconsistency in Toughness Evaluation of AISI 4340 Steel Austenitized at Increasing Temperatures", Metallurgical Transactions, Vol. 9A, 1978, pp. 331-341.

[7] Tetelman, A.S., Wilshaw, T.R., Rau, C.A., Jr., "The Critical Stress Criterion for Cleavage", International Journal of Fracture Mechanics, Vol. 4, 1968, pp. 147-156.

[8] Knott, J.F., "Macroscopic Aspects of Crack Extension", Advances in Elastic-Plastic Fracture Mechanics, Larsson, L.H., Ed., Applied Science Publishers, London, 1979, pp. 1 - 20

[9] Faucher, B., Tyson, W.R., Hong, Y., and Boutin, J., "Dependence of Ductile Fracture Toughness of a Weld Metal on Notch Root Radius and Inclusion Content", International Journal of Fracture, Vol. 46, 1990, pp. 173-184.

[10] Ritchie, R.O., Francis, B., and Server, W.L., "Evaluation of Toughness in AISI 4340 Alloy Steel Austenitized at Low and High Temperatures", Metallurgical Transactions, Vol. 7A, 1976, pp. 831-338.

[11] Mulherin, J.H., Armiento, D.F., and Markus, H., "The Relationship Between Fracture Toughness and Stress Concentrations Factors for Several High Strength Aluminum Alloys", Journal of Basic Engineering, Dec., 1964, pp. 709, 717.

[12] Yoda, M., "The Effect of Notch Root Radius on the J-Integral Fracture Toughness Under Modes I, II, and III Loadings", Engineering Fracture Mechanics, Vol 26, No.3, 1987, pp. 425- 431.

[13] Pandey, R.K., "Significance of Limiting (Equivalent) Tip Radius and Crack Tip Deformation for Cleavage Induced Fracture in Structural Steels", Journal of Materials Science, Vol. 19, 1984, pp. 607-614.

[14] Pratap, C.R., and Pandey, R.K., "Effect of Geometry and Finite Root Radius on Plastic Zone and Tip Opening Displacement", Engineering Fracture Mechanics, Vol. 19, No. 5, 1984, pp. 849-861.

[15] Swanson, R.E., Thompson, A.W., and Bernstein, I.M., "Effect of Notch Root Radius on Stress Intensity in Mode I and Mode III Loading", Metallurgical Transactions, Vol. 17A, 1986, pp. 1633-1637.

[16] Firrao D., Begley, J.A., De Benedetti, B., Roberti, R., and Silva, G., "Fracture Initiation and Propagation at the Root of the Notch in As-Quenched AISI 4340 Steel Charpy Type Bars with Varying Notch Root Radii", Scripta Metallurgica, Vol. 14, 1980, pp. 519-524.

[17] Zeman, J., Rolc, S., Buchar, J., and Pokluda, J., in "Fracture Mechanics: Twenty-First Symposium", ASTM STP 1074, ASTM, Philadelphia, 1990, pp. 396-418.

[18] Xiulin, Z., "On a Unified Model for Predicting Notch Strength and Fracture Toughness of Metals", Engineering Fracture Mechanics, Vol. 33, No. 5, pp. 685-695.

Table 1. Dimensions of three point bend bars (SENB) used for preliminary tests.

	Fatigue Precrack	EDM Notch
ρ	≈ 0	60 - 75 mm (0.0025 -0.003 in.)
W	50.8 mm (2.00 in.)	50.8 mm (2.00 in.)
B	24.3 mm (0.955 in.)	24.3 mm (0.955 in.)
B_{net}	20.3 mm (0.80 in.)	20.3 mm (0.80 in.)
a_o	30.1-30.5 mm (1.18-1.20 in.)	23.0 mm (0.906 in.)
a_o/W	0.59 - 0.60	0.45
Material:	Low alloy steel	
	(0.15 %C, 0.37 %Mn, 0.56 %Cr, 4.29 %Ni, 0.29% Mo)	

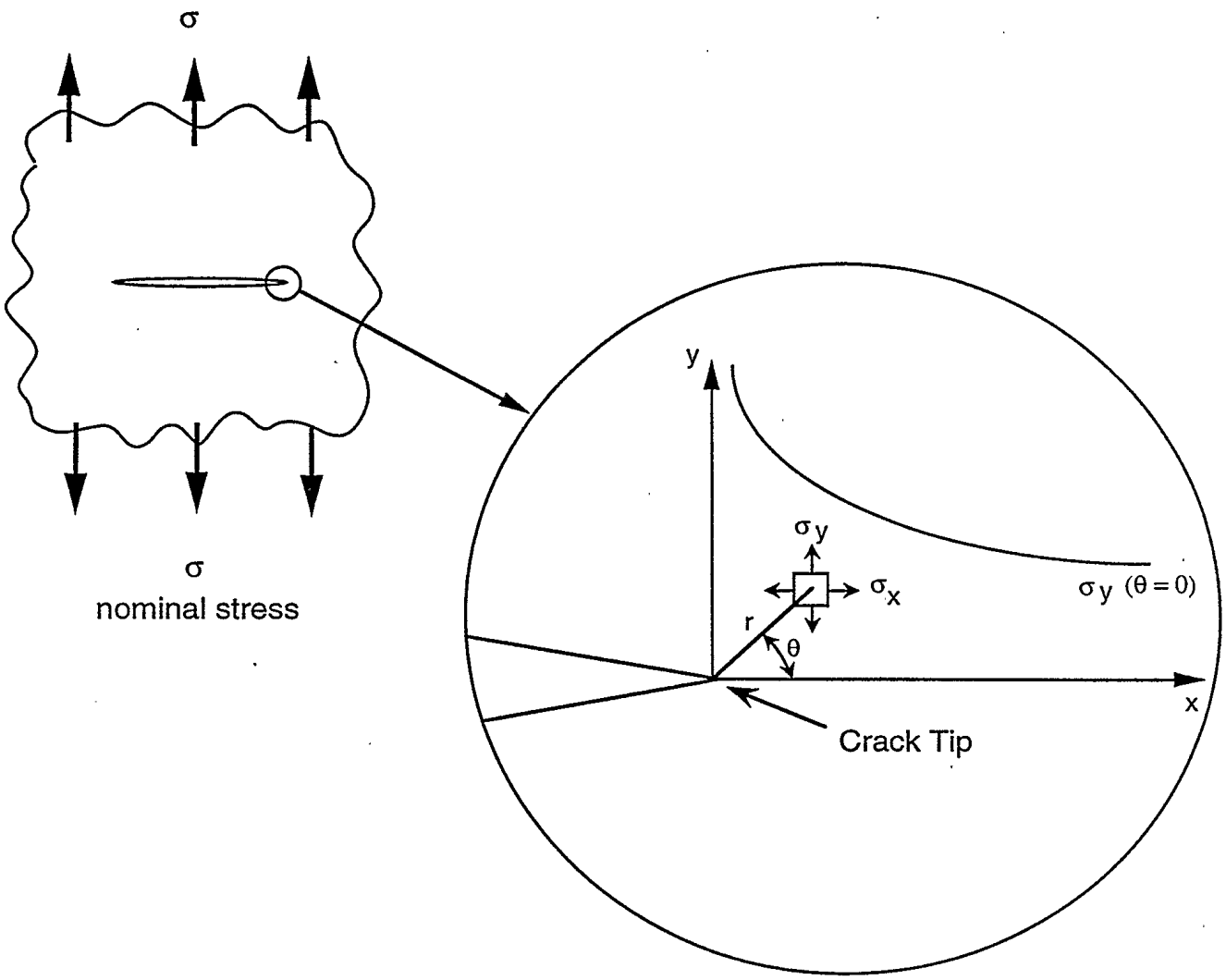

Figure 1. Illustration of the elastic stresses ahead of a fatigue crack.

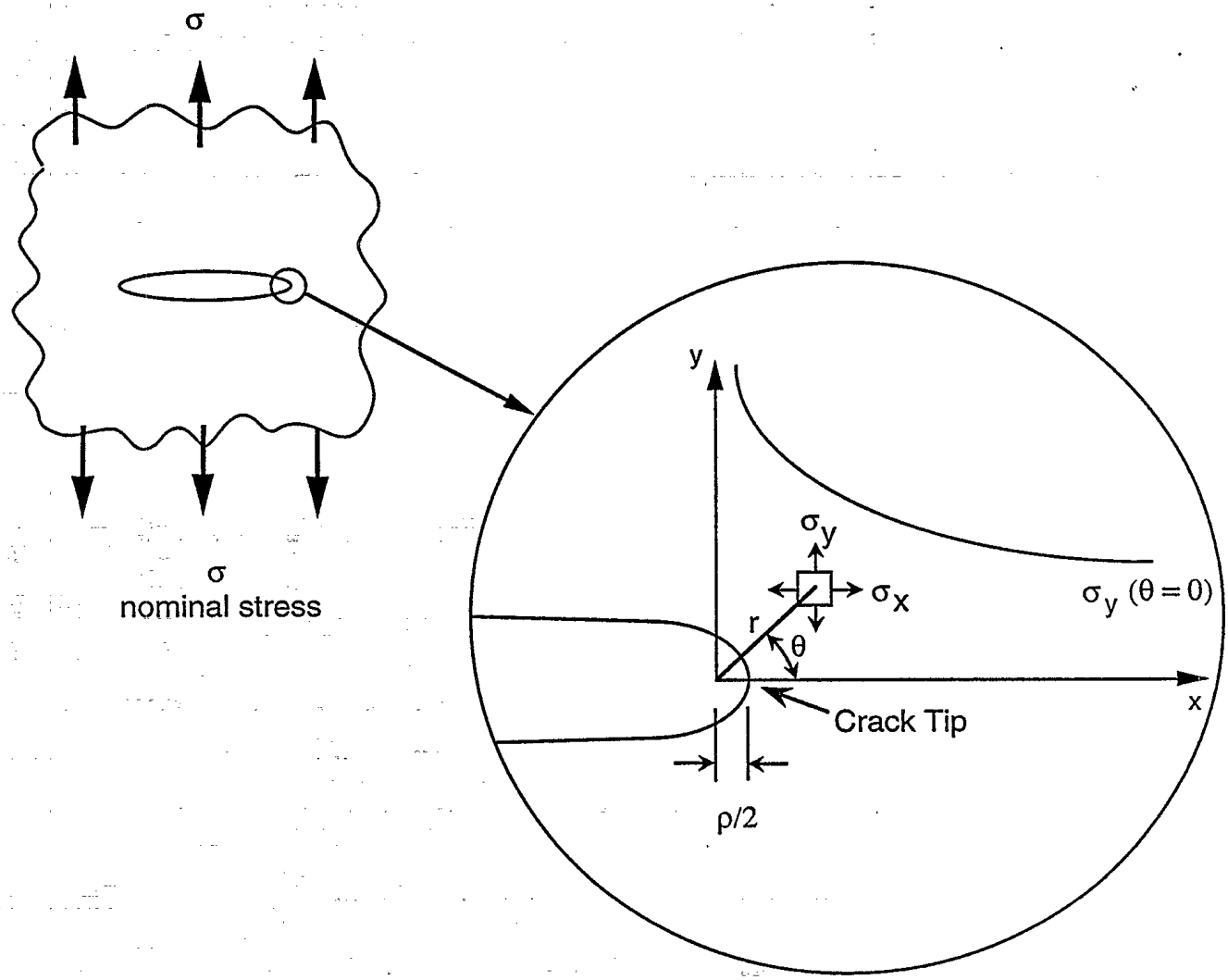

Figure 2. Illustration of the elastic stress distribution ahead of an elliptical notch with crack tip radius ρ.

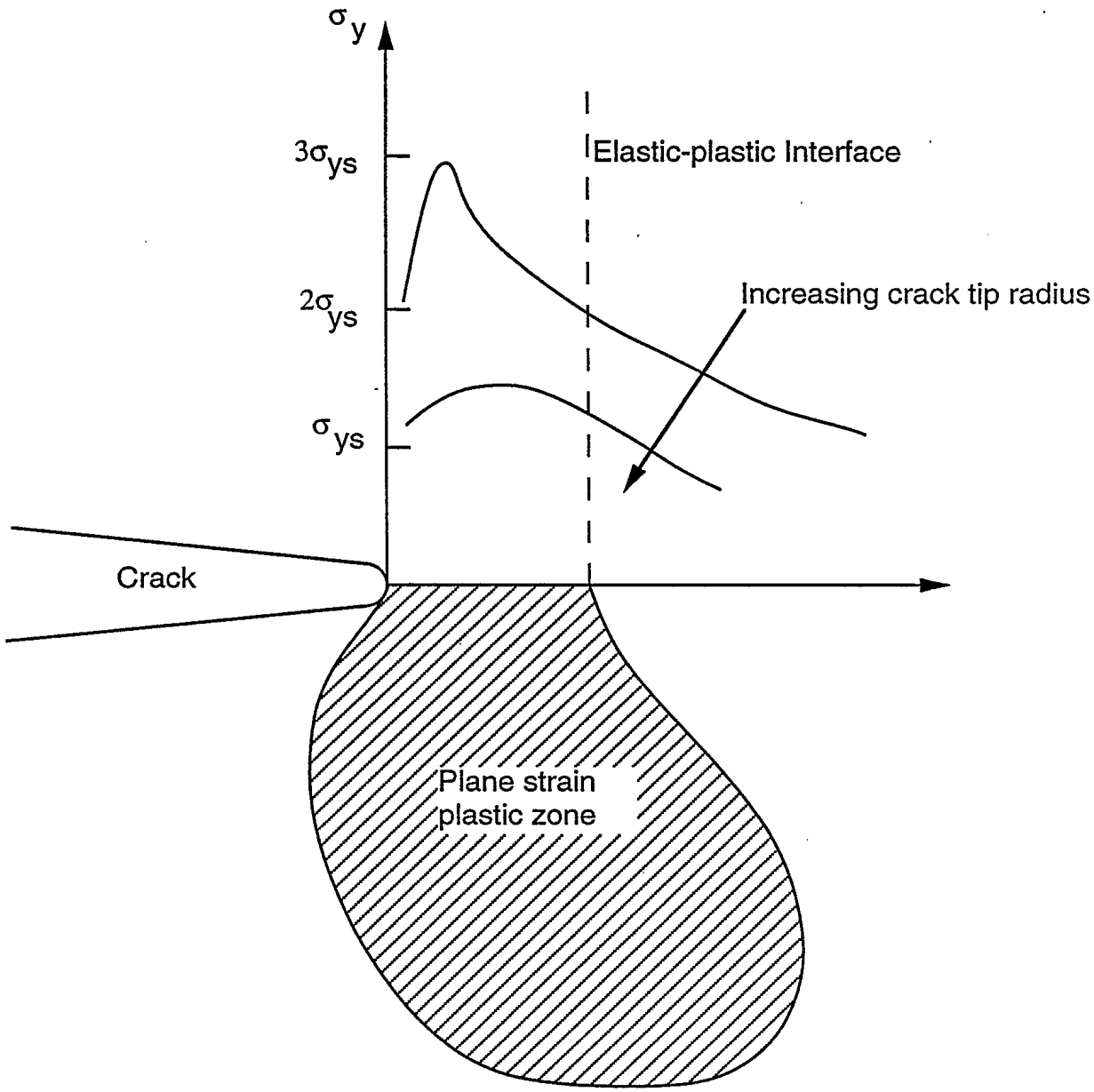

Figure 3. Illustration of the effect of increasing crack tip radius on the stress (σ_y) distribution ahead of the crack for a perfectly elastic-plastic material under plane strain conditions.

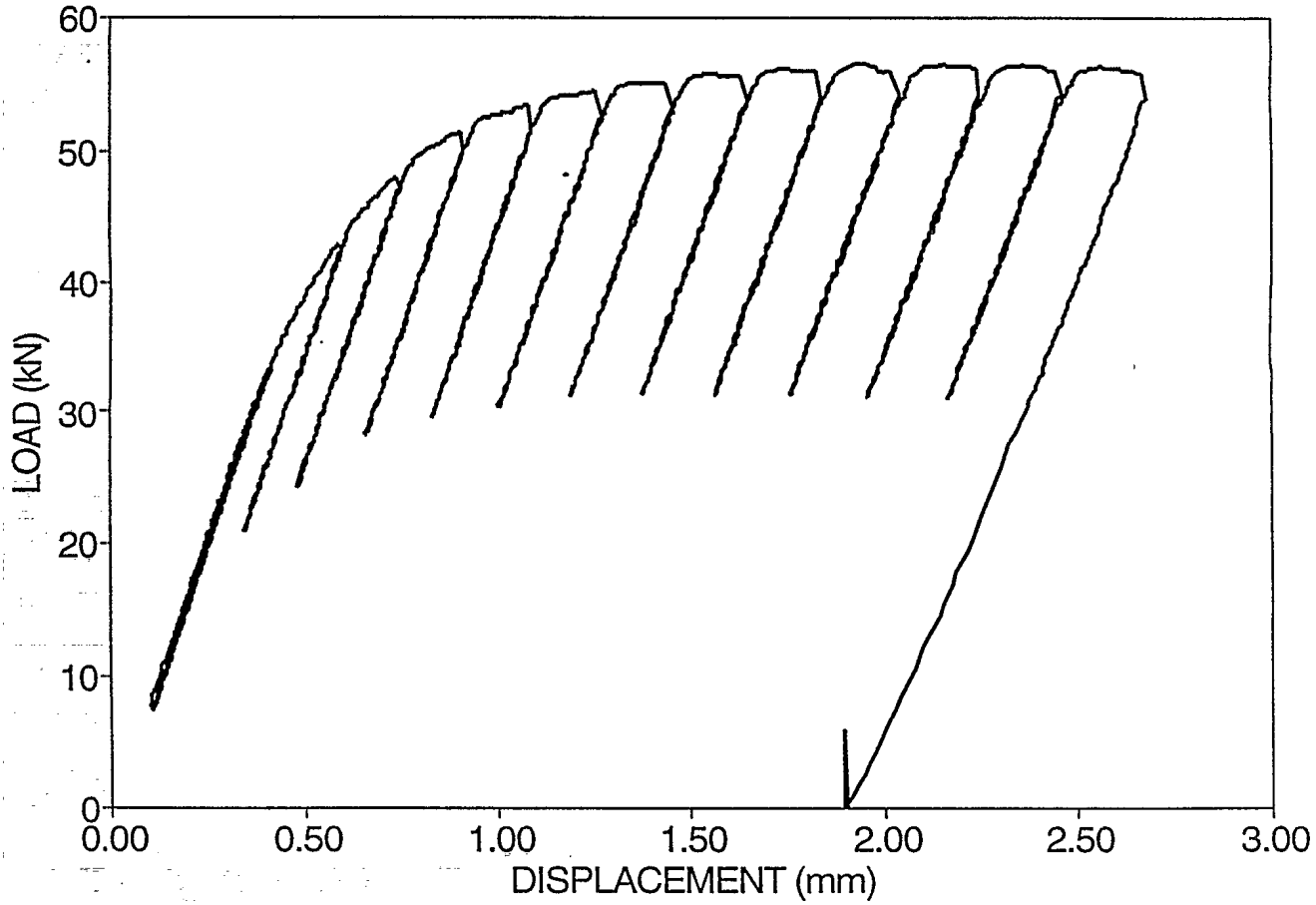

Figure 4. Typical load-displacement curve for a fatigue precracked specimen.

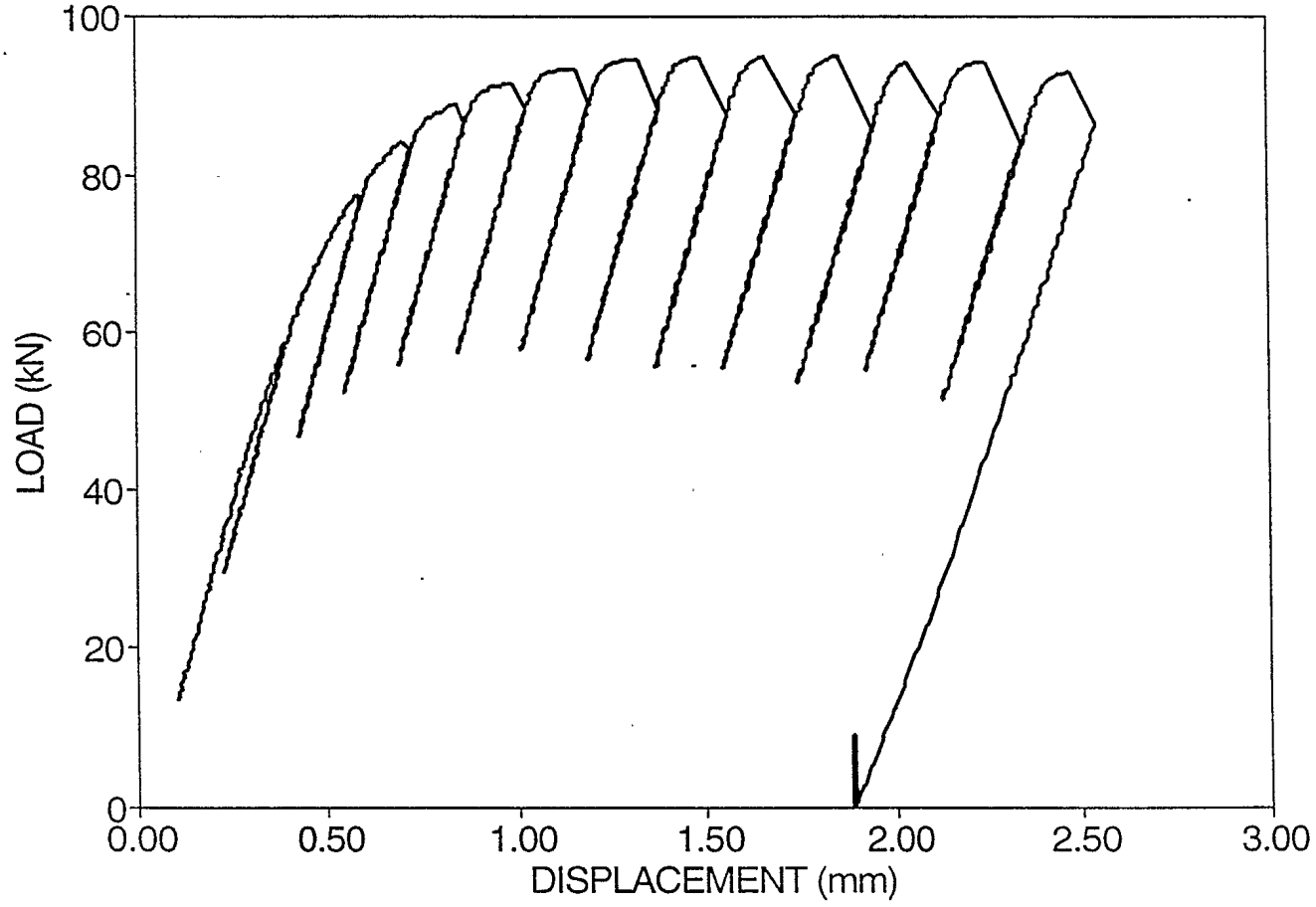

Figure 5. Typical load-displacement curve for an EDM notched specimen.

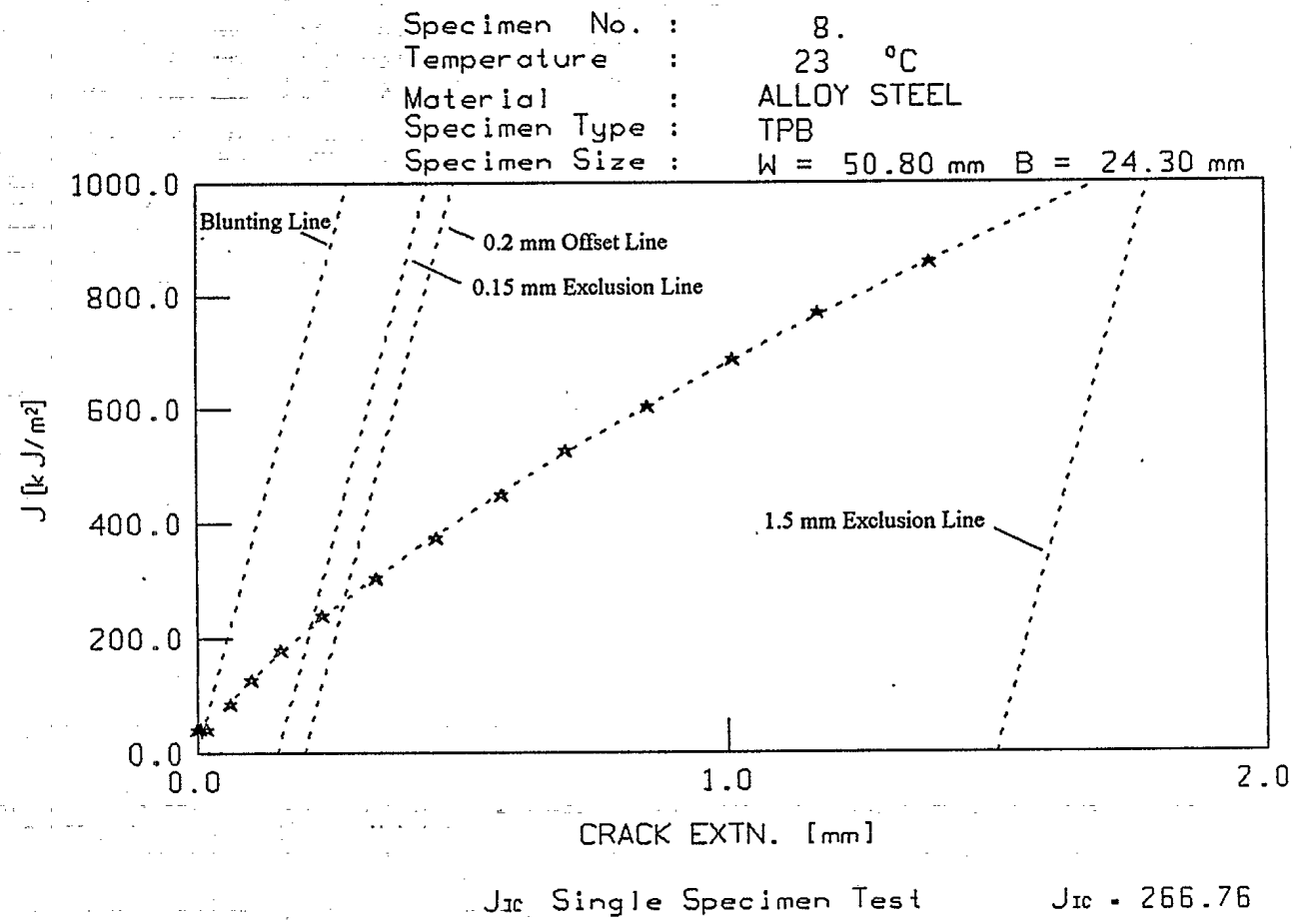

Figure 6. Typical J vs Δa curve for a fatigue precracked specimen.

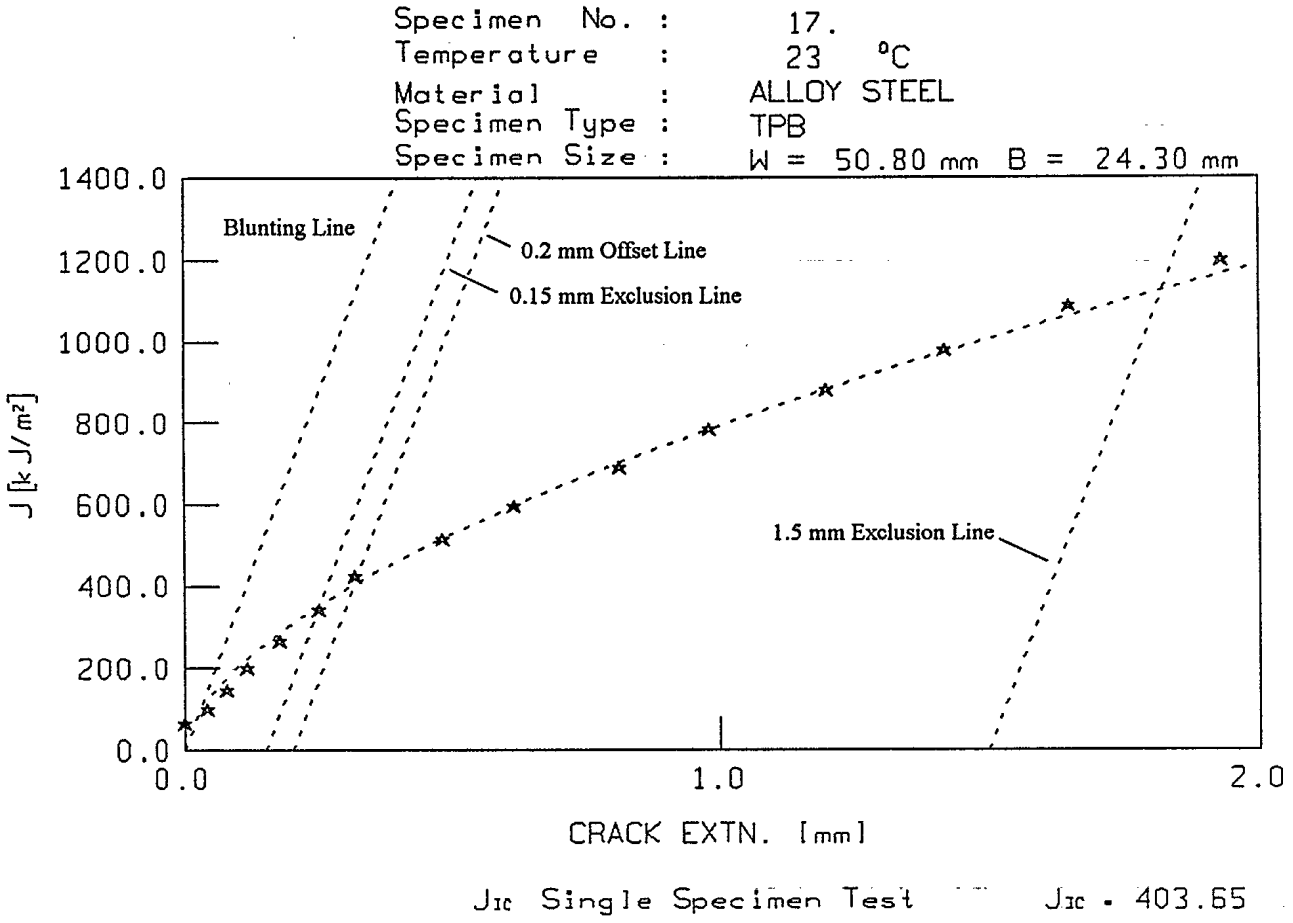

Figure 7. Typical J vs Δa curve for an EDM notched specimen.

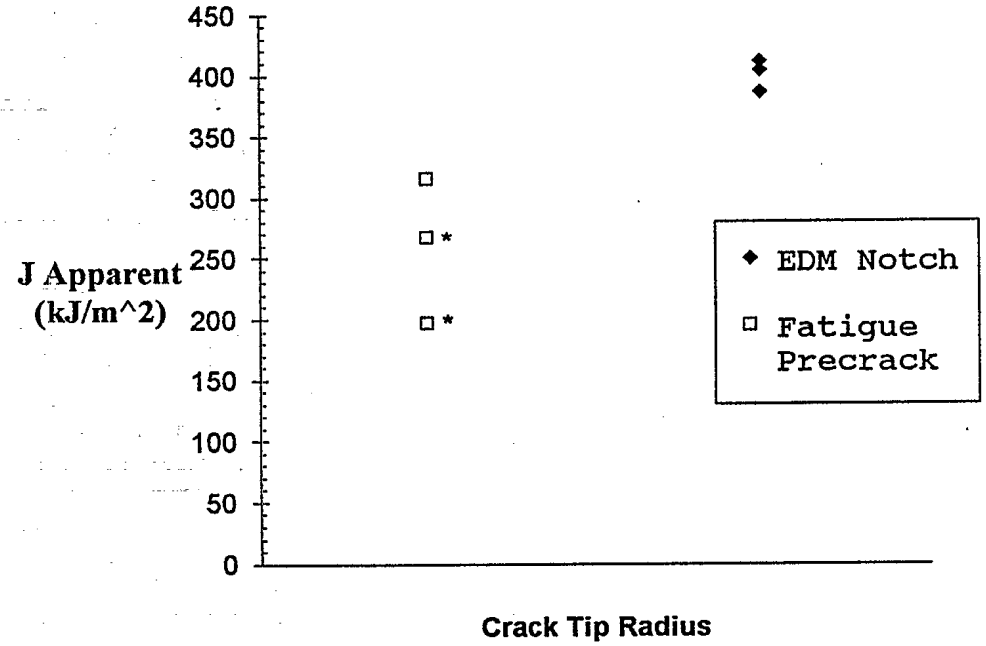

Figure 8. Apparent fracture toughness for the fatigue precracked and EDM notched specimens. (* valid J_{IC}).

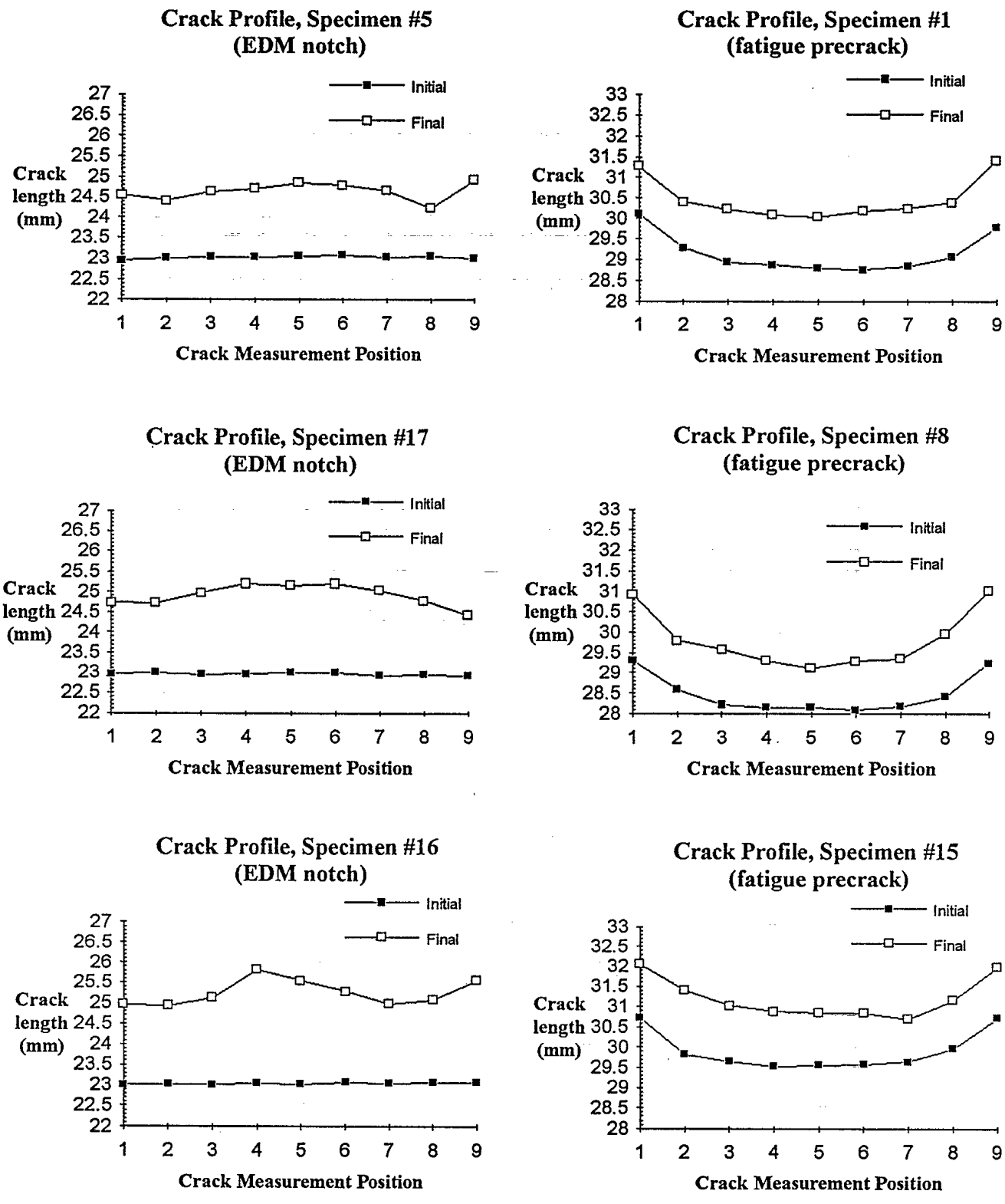

Figure 9. Initial and final crack profiles for the EDM notched and fatigue precracked specimens.